Changes in cerebral arterial pulsatility and hippocampal volume: a transcranial doppler ultrasonography study

Miller, Matthew; Ghisletta, Paolo; Jacobs, Bradley S; Dahle, Cheryl L; Raz, Naftali

How to cite

MILLER, Matthew et al. Changes in cerebral arterial pulsatility and hippocampal volume: a transcranial doppler ultrasonography study. In: Neurobiology of aging, 2021, vol. 108, p. 110–121. doi: 10.1016/j.neurobiolaging.2021.08.014

This publication URL: https://archive-ouverte.unige.ch/unige:163550
Publication DOI: 10.1016/j.neurobiolaging.2021.08.014

Neurobiology of Aging 108 (2021) 110–121

Contents lists available at ScienceDirect

Neurobiology of Aging

journal homepage: www.elsevier.com/locate/neuaging.org

Regular article

Changes in cerebral arterial pulsatility and hippocampal volume: a transcranial doppler ultrasonography study

Matt L Miller[a,*], Paolo Ghisletta[a,b,c], Bradley S Jacobs[d], Cheryl L Dahle[e], Naftali Raz[e,f,g]

[a] Université de Genève, FPSE, Genève GE, Switzerland
[b] UniMail, Swiss National Centre of Competence in Research LIVES, Genève GE, Switzerland
[c] UniDistance Suisse, Brig VS, Switzerland
[d] Wright State University, Department of Internal Medicine and Neurology, Dayton, Ohio
[e] Wayne State University, Institute of Gerontology, Detroit, Michigan
[f] Wayne State University, Department of Psychology, Detroit, Michigan
[g] Max Planck Institute for Human Development, Berlin-Dahlem, Germany

ARTICLE INFO

Article history:
Received 21 April 2021
Revised 6 August 2021
Accepted 19 August 2021
Available online 27 August 2021

Keywords:
Cognitive aging
Longitudinal growth curves
Cerebrovascular health
Arterial stiffness
Fluid intelligence
Transcranial Doppler

ABSTRACT

The physiological mechanisms of age-related cognitive decline remain unclear, in no small part due to the lack of longitudinal studies. Extant longitudinal studies focused on gross neuroanatomy and diffusion properties of the brain. We present herein a longitudinal analysis of changes in arterial pulsatility – a proxy for arterial stiffness – in two major cerebral arteries, middle cerebral and vertebral. We found that pulsatility increased in some participants over a relatively short period and these increases were associated with hippocampal shrinkage. Higher baseline pulsatility was associated with lower scores on a test of fluid intelligence at follow-up. This is the first longitudinal evidence of an association between increase in cerebral arterial stiffness over time and regional shrinkage.

1. Introduction

Performance on multiple cognitive tasks declines with age, even in healthy older adults (Horn, 1982; Park & Schwarz, 2000; Nyberg et al., 2020). Despite ample literature documenting this decline, the underlying neural mechanisms are unclear. The relationship between changes in the brain and cognition remains elusive (Raz, 2020), with almost every extant longitudinal study limited to investigation of structural properties of the brain (Daugherty & Raz, 2015; Fletcher et al., 2018; Bender et al., 2016; Yuan, Voelkle, & Raz, 2018).

1.1. Cognitive aging and cerebrovascular properties

Though the brain is 1 of the prime recipients of the body's blood supply (Attwell & Laughlin, 2001) and the brains of older adults show significant age-related vascular differences (Abdelkarim et al., 2019), the role of cerebrovascular changes in age-related cognitive decline is insufficiently explored. To date, the preponderance of evidence regarding cerebrovascular aging comes from cross-sectional studies. Although several cross-sectional comparisons between younger and older adults have shown that the latter have lower arterial cerebral blood flow (CBF[1]; Chen, Rosas, & Salat, 2011; Henriksen et al., 2014; Parkes et al., 2004; Shirahata et al., 1985; van Es et al., 2010; Zarrinkoob et al., 2015; Zhao et al., 2007; Raz et al., 2017), information about hemodynamic changes and individual differences in change is extremely sparse. Elucidating these temporal dynamics requires longitudinal studies (Raz & Lindenberger, 2011), without which, we cannot advance the understanding of change and individual differences therein (Lindenberger et al., 2011; Raz & Lindenberger, 2011).

The rare longitudinal investigations of CBF in older adults support the idea of age-related decline in arterial input to the brain (ten Dam et al., 2007) and differential declines in stationary re-

* Corresponding author at: Université de Genève, FPSE, Boulevard de Pont d'Arve 40, 1211, Genève GE, Switzerland, Tel: +41 (22) 379 81 77, FAX: +41 (22) 379 90 20.
E-mail address: matthew.miller@unige.ch (M.L. Miller).

[1] Abbreviations: CBF, cerebral blood flow; Gf, general fluid intelligence; LCS, latent change score; MR, metabolic risk; PI, pulsatility index; rCBF, regional cerebral blood flow; SEM, structural equation model; TCD, transcranial Doppler sonography.

0197-4580/$ – see front matter
https://doi.org/10.1016/j.neurobiolaging.2021.08.014

gional CBF (rCBF) to age-vulnerable regions (Beason-Held et al., 2008a, 2008b; MacInnes et al., 1989). Moreover, vascular risk indicators such as arterial hypertension, especially in people with long-term history of elevated blood pressure, are associated with age-related declines in rCBF within the circulation territories of all major cerebral arteries (Beason-Held et al., 2007). This supports the case for investigating major blood flow conduits of the brain in the context of cognitive aging.

Because endothelial dysfunction in cerebral vasculature has been hypothesized as the prime driver of age-related brain declines (de la Torre, 2008), investigations of age differences and changes in dynamic indicators of vessel stiffness over time are particularly cogent. Information about important aspects of brain hemodynamics within major cerebral vessels can be obtained from a widely accessible technique – transcranial Doppler (TCD) sonography (Naqvi et al., 2013). TCD can also be used to determine pulsatility index (PI; Gosling & King, 1974), which is defined as the ratio of the difference between peak systolic velocity and end diastolic velocity over average velocity. Because the systolic-diastolic velocity gap depends in part on the stiffness of the insonated vessel, PI can serve as a proxy for arterial stiffness (Park et al., 2013; Tarumi et al., 2014), and therefore as a marker of endothelial function.

Thus far, however, we know of only 1 longitudinal investigation of PI change, which found no association with changes in brain white matter hyperintensities (WMH) and did not examine regional gray matter volumes (Kneihsl et al., 2020). Other studies of PI change examine cross-sectional age differences in healthy adults, with no information available about individual differences in age-related PI change. Cross-sectional studies of broad-age-range community samples generally reveal higher PI in the major cerebral arteries of older participants (Bakker et al., 2004; Müller & Schimrigk, 1994; Sugimori et al., 1993), although not in all samples (Szolnoki et al., 2004). Cumulative cross-sectional evidence points to increased arterial pulsatility as an important indicator of vascular pathology and related conditions. In some studies, metabolic and vascular risk factors, e.g. hypertension and diabetes mellitus, were found to exacerbate age-related differences (Sugimori et al., 1993; ten Dam et al., 2007; Vernooij et al., 2008). Increased PI in the middle cerebral artery (MCA) has been linked to arterial calcification and diabetes mellitus (Park et al., 2013). Higher PI in vertebral arteries correlated with increased cerebral microbleeds in persons with cerebral small vessel disease (Chou et al., 2019). These findings buttress the validity of PI as an index of cerebrovascular health.

Importantly, elevated pulsatility may accompany reduced cognitive performance. E.g., increased PI in the circle of Willis has been linked to the emergence of Alzheimer's Disease (Roher et al., 2011) and higher PI predicts conversion to dementia 6 years later (Chung et al., 2017). Greater MCA PI has been associated with poorer cognitive performance in patients with cerebral small vessel disease (Petrenko et al., 2020) as well as asymptomatic older adults (Alwatban et al., 2020). Of particular relevance to our study, the association between higher PI and lower fluid (but not crystallized) intelligence has been reported in healthy older adults (Keage et al., 2015). More specifically, arterial pulsatility determined by MRI in the hippocampus and the parahippocampal gyrus correlates with episodic memory performance in older adults (Vikner et al., 2021). Together, these cross-sectional findings suggest arterial pulsatility measured by PI obtained via TCD may be an important marker of age-related changes in cerebral hemodynamics and concomitant cognitive declines. To the best of our knowledge, longitudinal assessment of PI change and its relation to cognitive performance is currently unavailable. Moreover, little is known about changes in arterial pulsatility over time in the context of healthy aging. Even more important are individual differences in change, until now overlooked. The understanding of these differences is important for elucidating the role of declining cerebrovascular system health.

Differential regional shrinkage of the brain and cortical thinning are also hallmarks of aging, even in the absence of overt disease and gross neuropathology (Raz, 2020). Longitudinal studies have linked loss of cerebral volume to increase in vascular risk (Raz et al., 2008; Debette et al., 2011; Pase et al., 2018). It stands to reason, therefore, that increases in arterial stiffness, a canonical marker of cerebral aging, will be coupled with regional shrinkage in age-sensitive brain regions. In addition, an important question is whether elevation in arterial stiffness predicts commonly-reported structural brain declines or vice versa.

1.2. Aims of the current study

In this study, we present a longitudinal investigation of hemodynamic characteristics reflective of age-related change in cerebral artery stiffness in the normal aging brain. Although TCD yields many hemodynamic indicators and allows insonation of multiple cerebral arteries, in this study we concentrated on PI as a proxy for arterial stiffness and selected cerebral arteries representing anterolateral and posterior circulation territories of the brain. Less focused approaches would be ill-advised in the modest sample available for this study. We also investigate the relationships between the increase in cerebral arterial stiffness and shrinkage of key age-sensitive brain regions.

We hypothesized that arterial stiffness would increase over time as indicated by increases in PI. We also hypothesized that PI elevation would be associated with greater cognitive decline, and that this association would be mediated by changes in the volumes of brain regions traditionally associated with higher cognitive activity. Specifically, we hypothesized that changes in PI would be associated with change in the volumes of the cerebellum (Cb), hippocampus (HC), and lateral prefrontal cortex (LPFC). Finally, we hypothesized that the decreases in fluid intelligence (Gf) associated with increases in PI might be due to the associated changes in regional brain volume as evidenced by changes in volume mediating the relationship between PI and Gf.

2. Methods

2.1. Participants and study design

Participants in this study were part of a cohort recruited for a longitudinal investigation of brain and cognitive aging in healthy, middle-aged and older adults; participant recruitment methods and complete sample characteristics are presented elsewhere (Raz et al., 2010, 2012; Daugherty & Raz, 2016; Bender et al., 2016). The current study is limited to the subsample of those participants that underwent TCD examination and only to measurements taken at waves 2 and 3 of the original study. These measurement occasions, referred to henceforth as time 1 and time 2, respectively, were separated by approximately 17 months on average (mean = 16.55, SD = 2.88). This subsample included 40 adults (60% female) aged 50 years or older (Table 1). We include a brief summary of participant recruitment and procedure below.

Participants were recruited from the Detroit metropolitan area by advertisement in local media. All had at least high-school education, English as the native language, and strong right-handedness. Persons with a self-reported medical history of or taking prescription medication to treat cardiovascular disease, neurological disorders, psychiatric conditions, diabetes, drug and/or alcohol abuse, thyroid problems, and head injury with loss of

Table 1
Descriptive statistics

	Time 1		Time 2	
Female (count)	24			
Male (count)	16			
White (count)	31			
Non-White (count)	9			
Age (yrs.)	65.26	(9.15)	66.66	(9.44)
Education (yrs.)	16.48	(2.68)		
Systolic BP (mmHg)	127.6	(10.8)	128.3	(12.4)
Diastolic BP (mmHg)	77.6	(7.6)	76.0	(6.4)
Body Mass Index	27.8	(4.5)	27.4	(4.6)
Fasting glucose (mg/dL)	90.9	(9.8)	88.2	(8.9)
Triglycerides (mg/dL)	121.5	(52.5)	125.2	(52.5)
Total cholesterol (md/dL)	212.5	(38.0)	209.3	(37.4)
HDL (mg/dL)	57.8	(12.8)	55.8	(14.8)
LDL (mg/dL)	130.3	(34.3)	128.6	(34.3)
Hematocrit (% × 100)	42.77	(3.57)	42.81	(4.52)
Left VA PI	1.09	(0.18)	1.04	(0.21)
Right VA PI	1.11	(0.23)	1.08	(0.25)
Left MCA PI	1.09	(0.24)	1.07	(0.18)
Right MCA PI	1.11	(0.23)	1.06	(0.20)
Left Cb volume (cm^3)	54.53	(6.27)	53.49	(5.90)
Right Cb volume (cm^3)	54.11	(6.03)	53.36	(5.85)
Left LPFC volume (cm^3)	9.59	(1.18)	9.67	(1.24)
Right LPFC volume (cm^3)	9.72	(1.27)	9.84	(1.41)
Left HC volume (cm^3)	2.92	(0.40)	2.81	(0.35)
Right HC volume (cm^3)	3.04	(0.34)	2.88	(0.29)
CFIT subscale 1 (correct items)	6.29	(1.56)	6.70	(1.80)
CFIT subscale 2 (correct items)	7.71	(1.59)	7.83	(2.00)
CFIT subscale 3 (correct items)	5.00	(1.45)	5.37	(1.07)
CFIT subscale 4 (correct items)	6.32	(1.45)	6.17	(1.72)

Note: Figures in parentheses are standard deviations where applicable, BP,blood pressure; HDL,high density lipids; PI,pulsatility index; VA,vertebral artery; MCA,middle cerebral artery; CFIT,Culture Fair Intelligence Test; Cb,cerebellum; LPFC,lateral prefrontal cortex; HC,hippocampus.

consciousness exceeding 5 minutes, including those taking antiseizure, anxiolytic, or antidepressant medication, were excluded. Participants were also screened for dementia and depression using the Mini-Mental State Examination (MMSE) (Folstein et al., 1975) and the Center for Epidemiological Studies Depression Scale (CES-D) (Radloff, 1977), with MMSE scores below 26 and/or CES-D scores above 15 as exclusion criteria. All participants provided informed consent. The study was approved by the Wayne State University Institutional Review Board.

Descriptive statistics for this sample can be found in (Table 1). With respect to lipid profile, 63% and 55% of the participants at time 1 and 2, respectively, had cholesterol in the dyslipidemic range. Arterial blood pressure assessed at the 2 measurement occasions revealed that 7% and 13% of participants at time 1 and 2, respectively, could be classified as hypertensive. None of the participants had fasting glucose levels in the diabetic range. Of the participants with available BMI, 32% and 33% met the criterion for (BMI $\geq$ 30) obesity at time 1 and 2, respectively. Only 1 participant at time 1 and 2 participants at time 2 reported current smoking. Most participants (77% and 67% at time 1 and 2, respectively) reported engaging in moderate exercise at least once a week. Note that the sample has a lower occurrence than the reported prevalence for Michigan, where most of the participants were recruited, of diabetes (10.2%; Centers for Disease Control and Prevention 2021), obesity (36.0%; Centers for Disease Control and Prevention 2021), and smoking (18.9%; Centers for Disease Control and Prevention 2021). Thus, despite some common age-related risk factors, most participants were healthy, normotensive adults with no evidence of diabetes or anemia.

The participants included in this study had low WMH burden (see Raz et al., 2012 for the details of WMH measurements). We found the median total WMH volume at baseline was 28.6 mm^3 (range 12.5 – 57.2 mm^3). For comparison, in 2 recent population studies, median WMH volumes were 997 mm^3 and 135.5 mm^3 (Grosu et al., 2021). Examination of FLAIR images revealed neither strokes nor objects that met the definition of lacunae outlined in the consensus paper on reporting cerebrovascular changes (Wardlaw et al., 2013).

3. Measures

3.1. Transcranial doppler ultrasonography: pulsatility index

Transcranial Doppler (TCD) ultrasound exam was performed with the 2 MHz Doppler DWL Multi-Dop P apparatus with version 2.2h operating software. The intracranial arterial vasculature, including middle cerebral, anterior cerebral, and posterior cerebral arteries, was insonated through the transtemporal windows; the internal carotid siphon and ophthalmic arteries through the transorbital window; and the vertebral and basilar arteries through the suboccipital window. The extracranial internal carotid artery was insonated through the submandibular window. The depth and angle of insonation that provided the waveform with the greatest mean flow velocity was used for analyses. Each artery was insonated until the greatest mean flow velocity attainable was acquired, with a minimum of 10 cardiac cycles per artery. The mean CBF velocity (CBFV) and PI (using Gosling's formula, noted above) were calculated by the DWL Multi-Dop.

An experienced technician acquired the sonographic data using a hand-held probe. The same technician conducted the TCD exam at both measurement occasions, using the same apparatus. Although no resting period before insonation was specified, the measurement started after the participants had been comfortably seated in the room for several minutes. The current literature shows that in measuring CBFV, handheld probes do not differ from frame-based devices and attain single-operator test-retest reliability of ICC=.80 (Saeed et al., 2012). In the sample reported on herein, composite reliability for PI exceeded .80 for all arteries insonated (see Online Supplemental Material for details). Descriptive statistics are shown in (Table 1).

Although TCD was performed on multiple cerebral and extracerebral arteries, given the limited sample size it was necessary to restrict the number of analyzed vessels to allow estimation of the analytical models while avoiding excessive comparisons and the ensuing Type I error inflation. We focused on two vessels most pertinent to our hypotheses: the middle cerebral and vertebral arteries (MCA and VA), representative of anterolateral and posterior cerebral circulation, respectively. These vessels were chosen because they are easily and accurately insonated and they provide the blood supply to the majority of the brain. Moreover, the hemodynamic changes in these arteries are frequently studied and are among the more accurate predictors of pathology (Sloan et al., 2004). We chose the vertebral arteries instead of the basilar artery to satisfy a constraint imposed by our modelling approach requiring at least 2 manifest variables (PI in left and right VA) for formation of latent factors (see below). Though obtaining PI in the posterior cerebral artery (PCA) would be desirable for examining the effects of hemodynamic change on HC volume, in exploratory analyses the data collected for this artery proved too ill-conditioned for further statistical modeling.

3.2. Regional brain volume

MRI was used to determine regional brain volume for participants. A single 1.5 Tesla Siemens Magnetom Sonata scanner (Siemens Medical Systems, Erlangen, Germany) was used to acquire all images at both baseline and follow-up. A 3D high-

resolution magnetization-prepared rapid gradient-echo sequence of 144 slices was acquired to provide imaging for regional volume measurement. Acquisition of the sequence took 7.41 minutes using echo time (TE) of 3.93 ms, repetition time (TR) of 800 ms, inversion time (TI) of 420 ms, field of view (FOV) of 192 × 192 mm, acquisition matrix of 256 × 256 mm, flip angle of 20°, and voxel size of 0.75 × 0.75 × 1.5 mm^3.

A complete description of image processing and extraction of volume measures are provided elsewhere (Raz et al., 2004, 2005, 2010). The temporal order of all participants' images were randomized by a member of the team not involved in tracing, thus blinding tracers to the acquisition time of specific images as well as to the demographic characteristics of the participants. Regional volumes were computed from measured areas of each region of interest (ROI). ROI measures had reliability in excess of 0.93 as measured by ICC(2), the intraclass correlation for random raters (Shrout & Fleiss, 1979). Three ROIs measured in the initial study were used in this research: the cerebellar hemispheres (Cb), the lateral prefrontal cortex (LPFC), and the HC.

Cb was traced on every coronal slice in which it was visible, including hemispheric gray and white matter, the corpus medullare, and the cerebellar tonsils (for details, see Raz et al., 2004). The vermis, superior medullary velum and fourth ventricle were excluded. Cerebellar white matter included the peduncles on the slices preceding the anterior vermis' appearance due to difficulty in distinguishing them from adjacent white matter, but caudally to that slice they were reliably excluded as they were easily distinguished from the cerebellar gray matter. Reliability for Cb volume was ICC(2)=0.99.

LPFC was traced on the 8-12 coronal slices in the posterior 40% of the distance between the genu of the corpus callosum and the front pole. Reliability for LPFC volume was ICC(2)=0.97.

HC, including CA1-CA4, the dentate gyrus, and the subiculum, was traced on continuous slices perpendicular to the long axis of the HC between the mammillary bodies and the slice that showed the fornices rising from the fimbria. Reliability for HC volume was ICC(2)=0.95.

3.3. Metabolic and vascular risk indicators

Factors reflecting metabolic risk (MR) have been associated with cardiovascular and cerebrovascular changes in aging adults (Bender & Raz, 2015; Ghisletta et al., 2019). Indicators such as blood glucose, high-density lipids (HDL, as a negative indicator), triglycerides, systolic blood pressure, and waist-hip ratio have been explored. For blood glucose and lipid profile (total cholesterol, HDL, LDL, and triglycerides), participants underwent venipuncture and provided 20 cc of blood after a 12-hour overnight fast. Whole blood glucose was assessed via the enzymatic oxidase method, and the lipid panel via the direct cholesterol oxidase/cholesterol esterase method.

3.4. Fluid intelligence

Fluid intelligence was measured by administering the Culture Fair Intelligence Test Form 3B (CFIT) (Cattell & Cattell, 1973). The CFIT has four subtests of 10 to 14 items of increasing difficulty. These nonverbal items test abstract reasoning and require participants to infer the rules needed to provide correct responses and are closely associated with working memory, as are many fluid intelligence tests (e.g., Kyllonen and Christal, 1990). The 4r subtests reflect various aspects of abstract reasoning. We administered the timed version of the tests, which limits the time available to solve problems and thus also entails processing speed. Descriptive statistics for CFIT in this sample are shown in (Table 1).

3.5. Data analysis

To test the hypothesized change in PI and Gf over time, we used the latent change score (LCS) model (McArdle & Nesselroade, 1994), a type of structural equation model (SEM; Kline, 2016). To summarize this technique, described in more detail below, these models essentially allow researchers to combine multiple measures of the same underlying construct into a single measurement with noise mathematically removed. When the construct is observed longitudinally, these essentially fully-reliable measurements can then be differenced in the same framework to provide an error-free indication of the change in the construct between occasions. The SEM framework further provides insight into change both at the sample level and how the change differs between individuals. This allows sensitive predictive models to be constructed even in the presence of measurement noise and individual differences in the constructs being modeled or in their change.

SEM has the advantage of estimating noise and other nuisance sources of variance in variables separately from reliable measurement variance of latent variables. Specifically, SEM allows the combination of multiple manifest measures (e.g., CFIT subtests) of the same latent construct (e.g., fluid intelligence) and the retention of only the shared information between the measures, thus eliminating variance that is not common to all of them (Kline, 2016). This is accomplished by the specification of *latent variables* derived from the observed manifest variables measured in the study. Latent variables can also be specified mathematically by combining other latent variables, as we will describe below. Because information that is not shared across multiple indicators of the same construct represents noise or error, the resulting latent variables are *error-free*, hence fully reliable.

SEM has been widely applied to longitudinal data, particularly via the addition of mean structure to the models that allows estimation of change in levels over time (Bollen & Curran, 2006). A major advantage of using SEM in longitudinal models is the ability to directly model changes occurring over time and, importantly, to estimate variance in change. LCS models, also known as latent difference score models (Ferrer & McArdle, 2010), are applied when research questions focus specifically on change between occasions and provide estimates of both mean change and variance in change. This is accomplished by creating new latent variables that capture the difference between measurements at pairs of time points. When one is interested in constructs represented by latent variables, the latent difference score can itself be the difference of these latent constructs, thereby directly modeling change as well as individual differences therein. In the current study, the ability of LCS models to analyze longitudinal data consisting of only 2 time points was also an advantage.

We took a 5-step approach to statistical analyses. First, we constructed and tested univariate[2] LCS models of PI as a time-dependent variable (see Fig. 1). Second, we constructed a univariate LCS model of fluid intelligence (Gf; see Figure S10) and linked the models of PI to the model of Gf in an overall bivariate[3] LCS model to determine if initial PI levels and change therein predicted follow-up levels and change in Gf. Third, we constructed a univariate LCS model of regional brain volume and linked the models of PI to the models of volume for regions supplied by the artery in a series of bivariate LCS models. Fourth, we linked the models of

[2] Univariate in the sense that only 1 construct is modeled, though technically the model includes multiple observed variables assessing the construct at 2 time points.

[3] Likewise, not bivariate in the strict sense that it only contains 2 observed variables, but instead that it is used to study the associations between initial values and change in 2 constructs, each assessed by multiple observed variables measured at 2 time points.

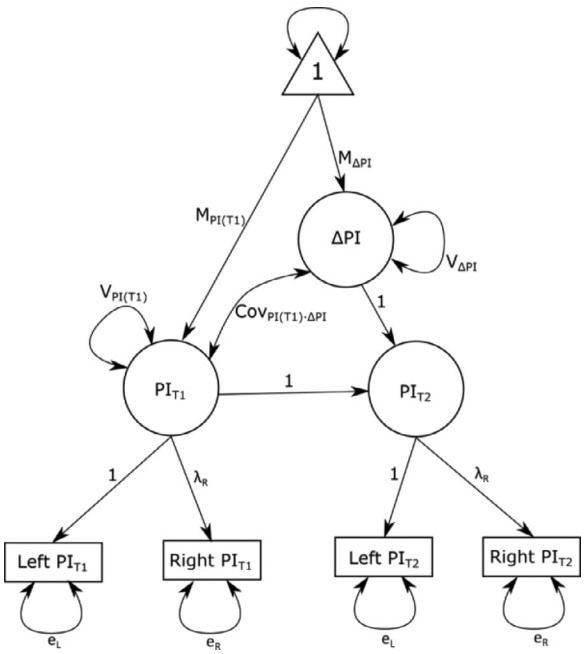

Fig. 1. LCS model for PI (the same model is used for volume, substituting "volume" for "PI"). Rectangles represent manifest variables; circles, latent variables; and the triangle, the constant one introducing mean structure. T1 indicates Time 1; T2, Time 2; *M*s are means, *V*s variances, *e*s unique variances, *Cov* covariance, and λ factor loadings.

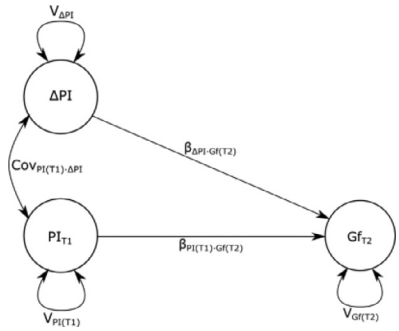

Fig. 2. PI-Gf latent variable model; only latent variables, their variance, covariance, and regressions are shown for clarity. Measurement models and mean structures are shown in Figure 1 for PI and Figure S10 for Gf. Standardized regressions are indicated by β. See Figure 1 for other notation conventions.

Gf to the models of regional volume in a separate series of bivariate LCS models. Finally, we constructed a model in which associations between PI, Gf, and volume were considered together in a trivariate LCS model. All statistical analyses were conducted in R (R Core Team, 2016) with the lavaan package (Rosseel, 2012). We used full-information maximum-likelihood estimation, which results in unbiased estimates in the face of data missing at random (Little et al., 2014). Our separate analyses showed that missing data were likely missing at random, thus satisfying this assumption (for details, see Online Supplemental Material).

In step one of the analyses, we evaluated LCS models to examine change in each artery's PI. LCS models assume that the same latent variable is assessed at both occasions, by constraining the same factor loadings (1 and λ_R) between the observed and the latent variables at both time points. Factor loadings are parameters that indicate the proportion of variance that a manifest variable contributes to the latent variable as compared to the reference manifest variable (the variable with a factor loading fixed to 1). Loadings also scale contributions of manifest variables' means to latent means. Then, the LCS model specifies the follow-up latent variable (PI_{T2}) as the sum of the baseline latent variable (PI_{T1}) and a latent variable, called ΔPI (in Fig. 1, $PI_{T2} = 1^{*}PI_{T1} + 1^{*}\Delta PI$). Thus, the latent variable ΔPI is defined as the difference between the latent assessments at the two time points (that is, $\Delta PI = PI_{T2}$ - PI_{T1}), thereby directly assessing the individual differences in change in the latent variable between baseline and follow-up. Note that the model does not calculate each participant's amount of change. Rather, it estimates the sample mean change ($M_{\Delta PI}$), the magnitude of individual differences in change (variance in ΔPI, $V_{\Delta PI}$), and the covariance between initial level and change ($Cov_{PIT1\text{-}\Delta PI}$). The model also estimates initial level statistics (mean amount, M_{PIT1}, and variance, V_{PIT1}). The major advantage of the LCS model is that initial level and change are estimated without measurement error (as both latent variables are defined after removal of error variance estimates e_L and e_R). Once we validated these models (see Online Supplemental Materials for details), we constructed LCS models for the latent PI variable in each artery (Fig. 1). Each of these models provided 5 parameter estimates of primary interest: the initial mean and the mean change (M_{PIT1} and $M_{\Delta PI}$, respectively), the initial variance and the variance in change (V_{PI1} and $V_{\Delta PI}$, respectively), and the linear association between initial level and change (the covariance $Cov_{PIT1\bullet\Delta}$). Because of our substantive focus on change, we were particularly interested in $V_{\Delta PI}$, which must be estimated to be significantly greater than zero if we are to test predictors of individual difference in change. Therefore, only LCS models for which $V_{\Delta PI}$ was significantly greater than zero were retained for testing of further models.

In step two, to determine if there were associations between PI and Gf, follow-up Gf was regressed on baseline PI and on change in PI for each artery (Fig. 2). This step began by constructing a univariate model of Gf. This model used time 2 (that is, the follow-up measurement, Gf_{T2}) as the anchor point instead of time 1 (Raz et al., 2008). That is, instead of defining a variable at baseline and another representing how much the construct changed at follow-up, we defined a variable at follow-up (Gf_{T2}) and another representing how much the construct had changed from baseline (ΔGf), such that $Gf_{T1} = Gf_{T2} - \Delta Gf$. We took this mathematically equivalent approach because we did not find significant change in Gf over time; that is, both mean ($M_{\Delta Gf}$) and variance ($V_{\Delta Gf}$) were statistically indistinguishable from zero. Given our interest in Gf as an outcome of PI, reparameterization of the model in this way allowed us to model individual differences in Gf at follow-up ($V_{Gf(T2)}$) so as to model associations with PI even though Gf did not change over time (see Online Supplemental Material for the complete LCS model of Gf). We then connected this univariate LCS model of Gf to the LCS model of PI, creating the bivariate model of interest for this step. We then tested covariance relationships among the latent variables and eliminated those that were not significant. Correlation between anchor-time measurements and change for both PI and Gf were also included.

In step 3, to determine if there were associations between PI and regional volume, we constructed a univariate LCS model of volume for each of Cb, HC, and LPFC. These models were configured in the same way as the LCS models of PI (Fig. 1), replacing PI with the volume of each region. We then connected this univariate LCS model of volume to the LCS model of PI for the artery supplying each region (VA for Cb and HC, MCA for LPFC), creating the bivariate model of interest for this step (Fig. 3). As in the previous step, we then eliminated paths that were not significant. Since the focus of this research was on hemodynamics, we only retained brain regions for which there were significant associations between PI and regional volume for further analyses.

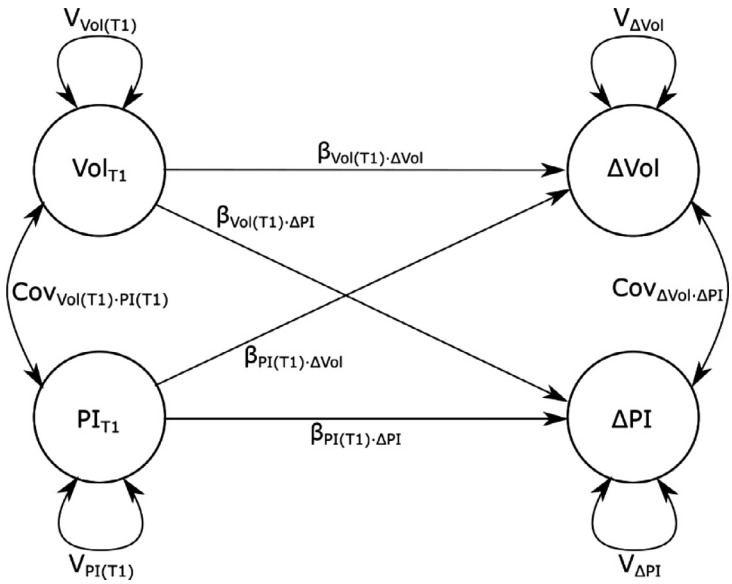

Fig. 3. PI-Volume latent-variable model; only latent variables, their variance, covariances, and regressions are shown for clarity. Measurement models and mean structures are shown in Figure 1 for PI and regional volume. Standardized regressions are indicated by β. See Figure 1 for other notation conventions.

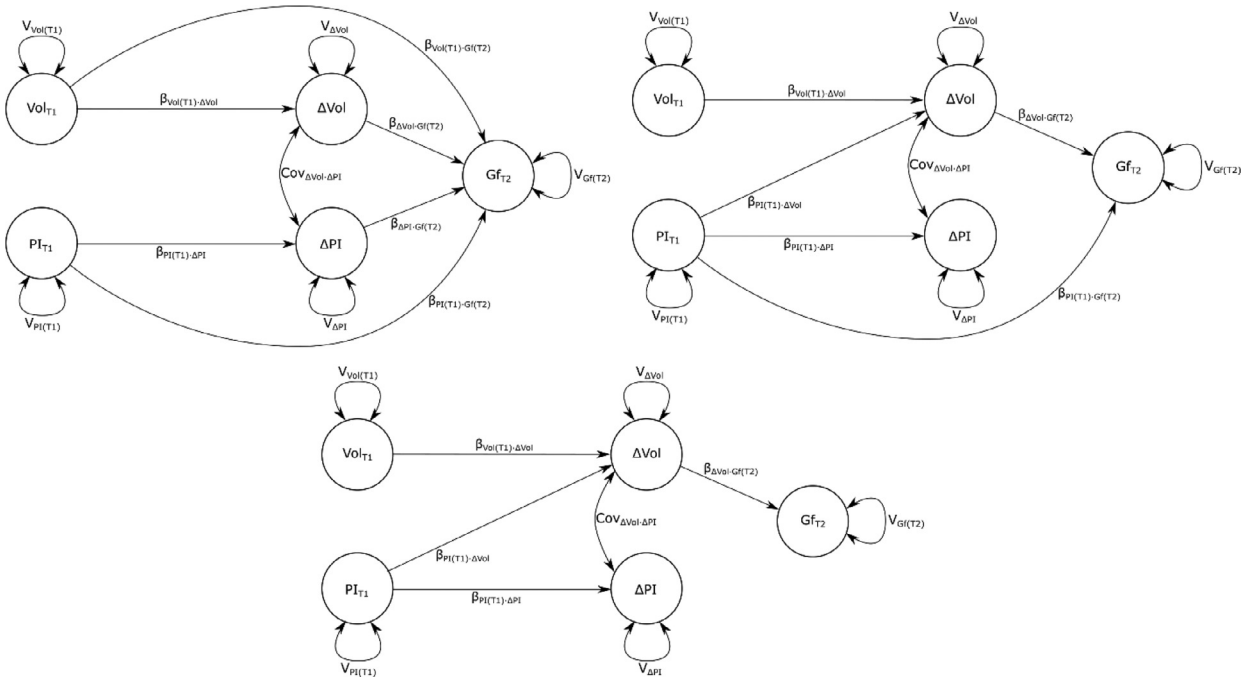

Fig. 4. Full PI-Volume-Gf models; only latent variables, their variance, covariances, and regressions are shown for clarity. Measurement models and mean structures are shown in Figure 1 for PI and volume and Figure S1 for Gf. Standardized regressions are indicated by β. Vol = regional volume; see Figure 1 for other notation conventions. Top left is complete model with initial volume and PI and change in volume and PI predicting Gf at follow-up; top right is model in which the effect of initial PI on Gf is partly mediated by change in volume, and bottom is model in which the effect of initial PI on Gf is fully mediated by change in volume.

In step four, we connected the univariate LCS model of volume to the model of Gf, using the same method as in step 2. As in that step, we only modeled relationships with Gf at follow-up since there was no variance in Gf change. As in previous steps, non-significant paths were eliminated.

Finally, in step 5, to determine if the associations of Gf with PI were mediated or moderated by volume or if the associations of Gf with volume was mediated or moderated by PI, we connected all 3 models. With this trivariate model, we tested initial level and change for both PI and volume as individual predictors, as partial mediators of predictors found in the bivariate models, and as full mediators of those predictors. Given our hypotheses, we were particularly interested in models in which regional volume mediated the associations between PI and Gf (Fig. 4).

To assess all models' statistical adequacy, we relied on several classical SEM goodness-of-fit indices that gauge a model's ability to reproduce the variance-covariance and mean structure of the data. We used χ^2 as a basis for rejecting models; confirmatory fit index (CFI) was used as a supplement to χ^2. As for tests of significance for model parameters, our cutoff threshold for χ^2 was set at a p-value of .05. That is, models with evidence of misfit that achieved $p \leq .05$ were rejected, as were nested models with likelihood ratio

Table 2
Estimates of interest for PI and Volume LCS models; bold indicates significant values

	Baseline mean (M_{T1})	Baseline variance(V_{T1})	Change mean (M_{Δ})	Change variance (V_{Δ})
PI, VA	1.083	0.026	-0.025	0.017
PI, MCA	1.097	0.048	-0.031	0.012
Volume, Cb	54.439	35.882	-1.054	3.015
Volume, LPFC	9.588	1.290	0.138	0.145
Volume, HC	2.931	0.101	-0.153	0.019

Note: PI,pulsatility index; VA, vertebral artery; MCA,middle cerebral artery; Cb,cerebellum; LPFC,lateral prefrontal cortex; HC,hippocampus.

χ^2 difference tests with a change in χ^2 that had $p \leq .05$. CFI values of less than .95 in combination with χ^2 p-value less than .10 (but greater than .05) were considered marginal, as were CFI values of less than .90 regardless of the χ^2 p-value. We examined the residual covariance matrix and parameter estimates for such models to determine if there were issues with a particular parameter or variable. When comparing models of association between constructs with more than two potential predictors, we also relied on the Bayesian information criterion (BIC) to indicate which model was both adequate as to fit and parsimonious as to the number of parameters.

2 participants had outlying values. 1 of these participants had a change in hematocrit at follow-up that was more than 3 standard deviations greater in absolute value than other participants, but whose values for all other measurements were well within the range of other observations. Another participant had combined CFIT subscale scores that were more than 3 standard deviations below that of other participants at baseline and more than 2.5 standard deviations below at follow-up. Because full-information maximum-likelihood estimation can use non-missing values in cases with some missing values to inform estimation of the overall model, instead of entirely eliminating these two participants from the analysis, only their anomalous measurements were set to "missing."

4. Results

Descriptive statistics for all observed variables are presented in (Table 1) (see Online Supplemental Materials for distributions, covariances, and longitudinal course of the observed variables). LCS models showed that PI in VA and MCA had variances in change, indicating individual differences in change (Table 2; see Online Supplemental Material for all estimates and p-values). Models including MR could not be supported due to absence of correlation between MR and PI in this sample. See the Online Supplemental Material for details, fit indices, and complete results.

Because mean change in PI was not significant, we set this parameter equal to zero ($M_{\Delta PI}$=0). When these models were refit, they were not statistically worse than the previous models with free parameters (VA PI: $\Delta\chi^2(1) = 0.792$, p =.373 and MCA PI: $\Delta\chi^2(1) = 1.614$, $p = .204$). We applied the same procedure to the Gf model with similar results ($\Delta\chi^2(1) = 0.477$, p =.490).

We proceeded to the next step in which PI at baseline and PI change predicted Gf at follow-up (Fig. 2). We found that only the regression path from baseline PI to follow-up Gf was significant (see Online Supplemental Material for details). Thus, the final model retained only this path (Fig. 5).

Baseline PI in both the VA ($\beta_{PI1.Gf2}$ = -0.639, $p = .001$) and the MCA ($\beta_{PI1.Gf2}$ = -0.439, $p = .017$) predicted Gf at follow-up, with higher PI foreshadowing lower Gf (Table 3; see Online Supplemental Material for fit indices and complete results).

We then proceeded to test associations between baseline PI, PI change, baseline regional volumes, and regional volume change (Fig. 3), controlling for age at initial assessment. Cb volume was several orders of magnitude larger than PI, therefore in the model containing both, PI was multiplied by 50 to bring variances to the same scale and to facilitate estimation. In that model, only HC had a significant association with PI in the supplying artery VA (Table 4; see Online Supplemental Material for fit indices and other estimates as well as the other 2 artery-region combinations). Specifically, change in VA PI was strongly negatively correlated with change in HC volume, such that individuals with increases in PI were likely to have proportional decreases in HC volume (correlation =-.706, $p = .028$). The model of associations between VA PI and Cb volume did not reveal significant associations and the model of associations between MCA PI and LPFC volume did not pass our goodness-of-fit requirements; therefore, these models were not evaluated further. We then compared models removing non-significant paths and found that the model with only the association between change in VA PI and change in HC volume was the most parsimonious (ΔBIC =-9.672) and did not fit significantly worse than the complete model ($\Delta\chi^2 = 1.395$, Δdf = 3, $p = .293$). This model revealed a slightly increased correlation between PI and regional volume; most other parameters were substantively unchanged.

Table 3
Parameters of interest for PI-Gf predictive models. All values are significant, indicated in bold

	VA PI – Gf	MCA PI – Gf
Regression of Gf T2 on PI T1	-3.615	-1.766
Standardized coefficient ($\beta_{PI(T1),Gf(T2)}$)	-0.639	-0.439
Mean baseline PI	1.079	1.067
Variance baseline PI	0.026	0.048
Variance change PI	0.016	0.013
Mean follow-up Gf	10.283	8.165
Variance follow-up Gf	0.494	0.663

We then tested associations between regional volume in HC and Gf, controlling for age at initial assessment. These models suggested that baseline HC volume and change in HC volume were both associated with Gf at follow-up, even when controlling for the correlation between baseline volume and volume change (Table 5; see Online Supplemental Material for complete model results and comparisons). However, these models all failed our goodness-of-fit criteria ($\chi^2(76) = 104.944$, $p = .016$; CFI = .869) and thus the results must be considered tenuous; we did, however, use the associations suggested by the final model to inform our exploration at the final step.

In our final analysis, we combined VA PI, HC volume, and Gf at follow-up into a single model, testing initial values and change in PI and volume for associations with Gf. As noted in the methods, we tested all four predictors (initial PI, PI change, initial volume, and volume change) together and individually, including combinations suggested by the results from the previous steps in our analysis, and specifically tested our hypothesis that regional volume mediated the association between PI and Gf. However, none of these

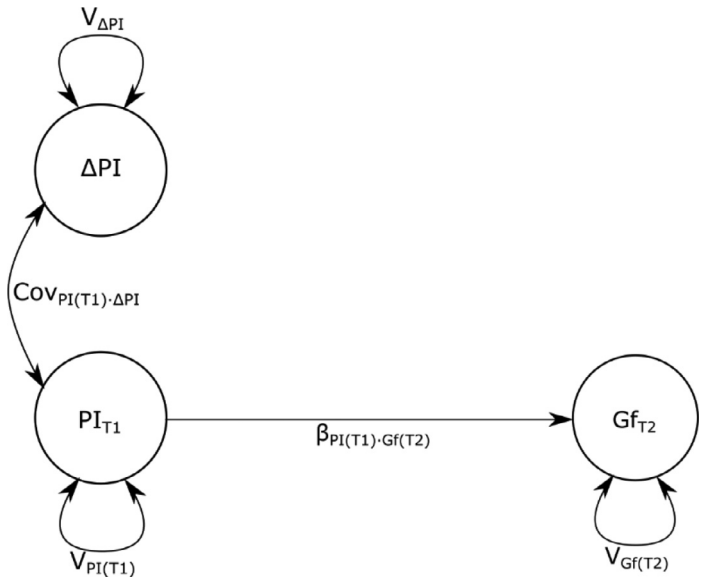

Fig. 5. Final latent variable model of PI and Gf. Path $Cov_{PI(T1)\bullet\Delta PI}$ is only estimated for MCA; it is fixed at zero for VA. Standardized regression is indicated by β. See Figure 1 for other notation conventions.

Table 4
Parameters of interest for VA PI-HC volume predictive model. Bold indicates significant values

	Complete model	Only ΔPI – Δvolume
Regression of Δvolume on PI T1	-0.261	
Standardized coefficient ($\beta_{PI(T1)\bullet\Delta Vol}$)	-.308	
Regression of ΔPI on volume T1	0.002	
Standardized coefficient ($\beta_{Vol(T1)\bullet\Delta PI}$)	.005	
Correlation of volume & PI at T1 ($Cov_{Vol(T1)\bullet PI(T1)}$)	-.058	
Correlation of volume & PI change ($Cov_{\Delta Vol\bullet\Delta PI}$)	-.706	-0.738
Mean PI T1	1.085	1.085
Variance PI T1	0.014	0.014
Variance change PI	0.017	0.017
Mean volume T1	2.922	2.922
Variance volume T1	0.076	0.076
Mean volume change	1.060	0.798
Variance volume change	0.010	0.011

Table 5
Parameters of interest for HC volume-Gf predictive model. Bold indicates significant values. Note that this model does not satisfy goodness-of-fit requirements

	Estimate
Regression of Gf T2 on volume T1	2.275
Standardized coefficient ($\beta_{Vol(T1),Gf(T2)}$)	.778
Regression of Gf T2 on volume change	4.431
Standardized coefficient ($\beta_{\Delta Vol,Gf(T2)}$)	.701
Mean volume T1	2.926
Variance volume T1	0.076
Mean volume change	0.843
Variance volume change	0.011
Mean Gf T2	0.477
Variance Gf T2	0.442

models passed our goodness-of-fit criteria (see Online Supplemental Material for complete model results and comparison). Nonetheless, we report here the most parsimonious model as it is suggestive for future research (Table 6). These results suggest that the effect of PI on Gf is not mediated by HC volume though initial PI remains significantly predictive of follow-up Gf; the strong association between change in PI and regional volume change is also retained (Figure 6).

Given the small sample size, we decided *post hoc* to ensure that the observed effects did not reflect the undue influence of a few extreme values. Therefore, we ran 1000 bootstrap replications of the final model, and found that the estimate of the covariance of change in VA PI with HC volume remained stable (mean=-0.010, 95% CI=(-0.022, -0.001)). The association between baseline VA PI and Gf at follow-up, estimated as -3.505, was slightly less robust since its 95% confidence interval included zero, CI=(-7.503, 0.381). However, only 4% of the bootstrapped estimates were greater than or equal to zero, speaking in favor of a negative relation between baseline VA PI and follow-up Gf. We thus consider the result reportable with the caveat that this association should be further explored in larger samples.

5. Discussion

In this study, we investigated changes in cerebral artery pulsatility, a proxy for arterial stiffness; in regional brain volume; and in cognitive performance in middle-aged and older adults over a relatively short span of approximately 17 months. We hypothesized that arterial stiffness would increase over time, that PI increases would be positively associated with cognitive decline and with regional volume change, and that the association of PI with cognitive decline would be mediated by regional volume change.

Table 6
Parameter estimates for final model. Standardized values (Std Est) for regression weights (β weights) and covariances (correlations) are given. Proportion of variance explained by the model (R^2) is shown with each variable's estimated unexplained variance. Bold indicates significant values

	Estimate	Std Est	R^2	p
Regression of Gf T2 on PI T1 ($\beta_{PI(T1)\bullet Gf(T2)}$)	-3.828	-0.677		.016
Covariance Δvolume with ΔPI ($Cov_{\Delta Vol\bullet\Delta PI}$)	-0.010	-0.743		.020
Mean Gf T2	10.524			<.001
Variance Gf T2	0.501		.400	.017
Mean PI T1	1.084			<.001
Variance PI T1	0.014		.467	.001
Variance ΔPI	0.016		.016	.007
Mean volume T1	2.922			<.001
Variance volume T1	0.076		.218	<.001
Mean Δvolume	0.769			.002
Variance Δvolume	0.011		.397	.015

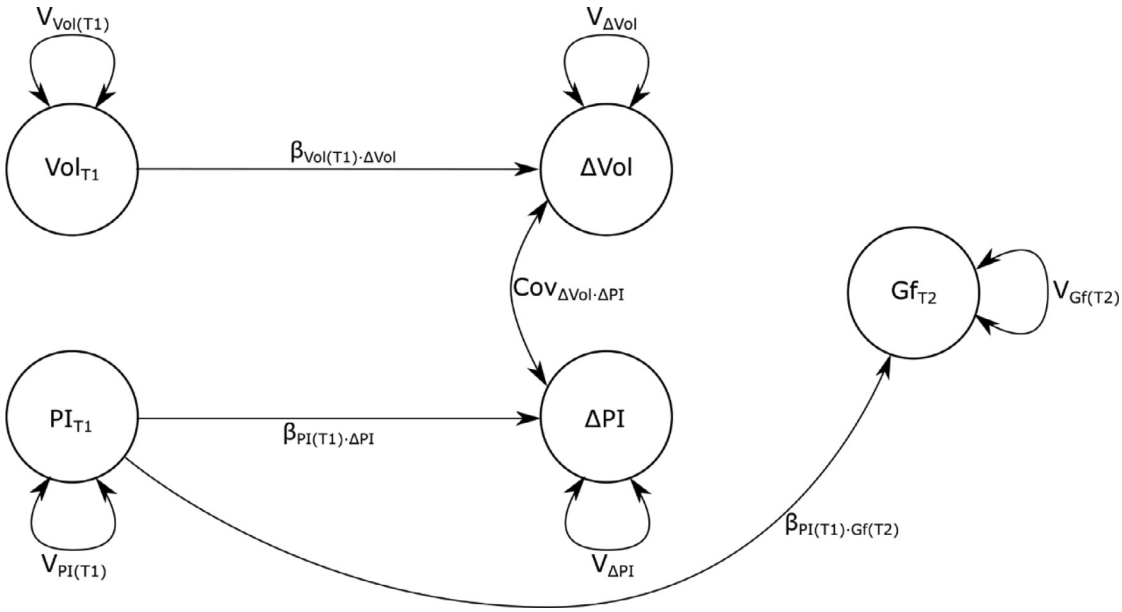

Fig. 6. Final latent variable model of VA PI, HC volume, and Gf. Standardized regression is indicated by β. See Figure 1 for other notation conventions.

In accord with our first hypothesis, we observed significant individual variability in PI change over time in VA and MCA. The mean change was minimal, as expected for such a short follow-up period (17 months), but though the majority of individuals experienced a drop in PI and some remained stable, a handful showed significant PI increase. Notably, change in the PI in the vertebral arteries was associated with shrinkage in one of the brain regions supplied by downstream tributaries of VA, the hippocampus (Fig. 7). Specifically, those who evidenced elevation in PI, presumably due to increase in arterial stiffness, also experienced the most reduction in hippocampal volume. Contrary to our expectations, no similar coupling was observed between the vertebral pulsatility and cerebellar shrinkage or between pulsatility change in the MCA and shrinkage in LPFC.

The hypothesized association between arterial stiffening and cognitive performance was only partially supported. Individual differences in PI change were unrelated to change in fluid intelligence. However, elevated baseline PI, reflecting pre-existing arterial stiffness, predicted lower fluid intelligence at follow-up. That relationship was not mediated by hippocampal shrinkage or by participants' age. This finding accords with the reports of PI as a predictor of cognitive declines (Chung et al., 2017), as well as a correlate of Gf (Keage et al., 2015) and episodic memory (Vikner et al., 2021).

The association found only between hippocampal shrinkage and stiffening of the vascular system that irrigates that region stood out among our findings, particularly since other hypothesized couplings provided null results. Although the reasons for this narrow finding are unclear, it is possible that arterial stiffening acted as an early harbinger of more widespread future pathology. This may be because the hippocampus as the most sensitive structural predictor of impending neurodegeneration may be the only structure to reveal association in these changes over a short follow-up period with a limited number of participants. Further, in the healthy adults comprising our sample it is plausible that only the hippocampus was sensitive enough to vascular decline to evidence shrinkage. Studies with a longer follow-up and a larger and more neurologically diverse sample might allow the detection of more widespread links between arterial stiffness and loss of volume in the areas irrigated by those arteries. Such findings would be consistent with reports linking arterial stiffness to cognitive deficits in persons with subjective memory complaints (Hanon et al., 2005) and asymptomatic older adults from community samples (Suri et al., 2020).

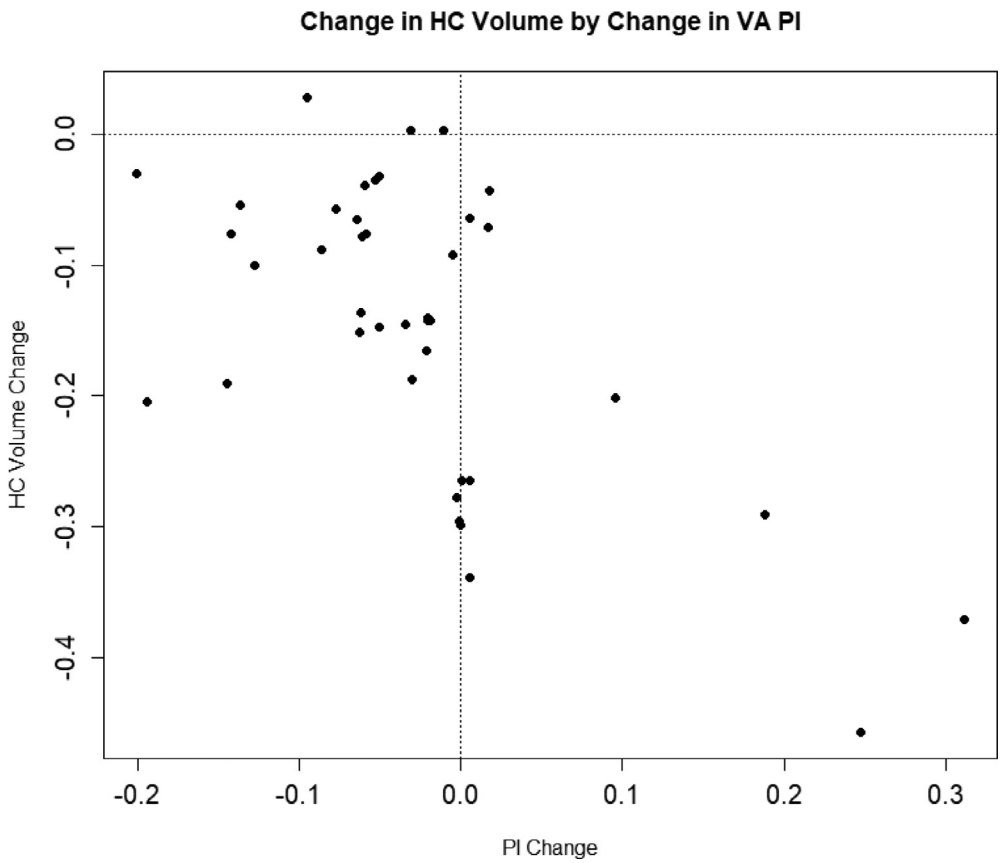

Fig. 7. Estimated latent factor scores for HC volume by VA PI, controlling for age. Dashed lines are at zero estimated change. Note that the apparently extreme observations did not drive the reported association between volume and PI, as confirmed by bootstrap replication.

The limitations of our study impose constraints on interpretation of its results. Statistical power was limited and therefore only strong effects could be observed with the customary level of confidence. Collecting data on only two occasions precluded ascertaining the lead-lag order of cerebrovascular, structural, and cognitive change. An intriguing set of hypotheses was not addressed in this study, in part for the lack of relevant measurements and in part due to limitations on the number of parameters that could be reasonably introduced into the models based on such a modest sample. E.g., the relationship between arterial stiffness and white matter properties within specific vascular territories is of great interest for elucidating age-related cerebral and cognitive declines. The relationships between higher PI and unfavorable white matter diffusion properties reported in cross-sectional studies (Fleysher et al., 2018) make this direction of research particularly intriguing. Assessment of PI would also be useful for providing more precise information about the effect of hemodynamic change on HC volume, as PCA is a more proximal source of HC vascularization than VA. However, the PCA data collected in this sample were not amenable for satisfactory statistical modeling. These limitations should be addressed in future studies.

In summary, in this longitudinal study of brain hemodynamics in a sample of healthier-than-average, middle-aged and older adults, arterial stiffness increased within a relatively short period. Moreover, the individual differences in arterial stiffening were robustly coupled with hippocampal shrinkage. We replicated a previously reported cross-sectional association between elevated PI and lower fluid intelligence. We have added to the understanding of this effect by showing that this association does not seem to be mediated by regional volume change in the HC. We have also found that those who have greater arterial stiffness at baseline were more likely to show reduced fluid intelligence at follow-up, demonstrating that this difference is persistent across time.

Finally, our findings raise an intriguing question of whether the age-related changes in the brain structure and cognition can be alleviated by intervention that mitigates cerebral arterial stiffening. There are grounds for optimism as it has been demonstrated that a brief aerobic training intervention dampens pulsatility increase in response to acute bouts of exercise in a small sample of healthy middle-aged and older adults (Akazawa et al., 2018). Thus, reduction of arterial stiffness may serve as an indicator of the benefits of aerobic exercise programs linked to the mitigation of cognitive decline (Hillman et al., 2008).

6. Data availability

All data, including access to public domain imaging data and R code used for analyses, is available at https://osf.io/x6umf.

Disclosure statement

The authors have no competing interests to declare.

This study was supported by NIA grant R03-AG024630 (NR, all data collection), by the European Commission, Horizon2020 under grant agreement number 732592-Lifebrain-H2020-SC1-2016-2017/H2020-SC1-2016-RTD (MLM, PG), and by NIH grant R01-AG011230 (NR).

Acknowledgements

We extend our thanks to Kent Agee for his expertise in conducting TCD examinations which was vital to the successful completion of this project. We would also like to thank the participants without whom this research would not have been possible.

Supplementary materials

Supplementary material associated with this article can be found, in the online version, at doi:10.1016/j.neurobiolaging.2021.08.014.

References

Abdelkarim, D., Zhao, Y., Turner, M.P., Sivakolundu, D.K., Lu, H., Rympa, B., 2019. A neural-vascular complex of age-related changes in the human brain: anatomy, physiology, and implications for neurocognitive aging. Neurosci Biobehav R 107, 927–944. doi:10.1016/j.neubiorev.2019.09.005.

Akazawa, N., Tanahashi, K., Kosaki, K., Ra, SG., Matsubara, T., Choi, Y., Zempo-Miyaki, A., Maeda, S., 2018. Aerobic exercise training enhances cerebrovascular pulsatility response to acute aerobic exercise in older adults. Physiol. Rep 6, e13681. doi:10.14814/phy2.13681.

Alwatban, M.R., Liu, Y., Perdomo, S.J., Ward, J.L, Vidoni, E.D., Burns, J.M., Billinger, S.A., 2020. TCD cerebral hemodynamic changes during moderate-intensity exercise in older adults. J. Neuroimaging 30, 76–81. doi:10.1111/jon.12675.

Attwell D & Laughlin, S.B., 2001. An energy budget for signaling in the grey matter of the brain. J. Cereb. Blood Flow Metb 21, 1133–1145. doi:10.1097/00004647-200110000-00001.

Bakker, S.L., de Leeuw, F.E., den Heijer, T., Koudstaal, P.J., Hofman, A ., Breteler, M.M., 2004. Cerebral haemodynamics in the elderly: the Rotterdam study. Neuroepidemiology 23, 178–184. doi:10.1159/000078503.

Beason-Held, L.L., Kraut, M.A., Resnick, S.M., 2008a. I. Longitudinal changes in aging brain function. Neurobiol. Aging 29, 483–496. doi:10.1016/j.neurobiolaging.2006.10.031.

Beason-Held, L.L., Kraut, M.A., Resnick, S.M., 2008b. II. Temporal patterns of longitudinal change in aging brain function. Neurobiol. Aging 29, 497–513. doi:10.1016/j.neurobiolaging.2006.11.011.

Beason-Held, L.L., Moghekar, A., Zonderman, A.B., Kraut, M.A., Resnick, S.M., 2007. Longitudinal changes in cerebral blood flow in the older hypertensive brain. Stroke 38, 1766–1773. doi:10.1161/STROKEAHA.106.477109.

Bender AR & Raz, N., 2015. Normal-appearing cerebral white matter in healthy adults: mean change over 2 years and individual differences in change. Neurobiol. Aging 36, 1834–1848. doi:10.1016/j.neurobiolaging.2015.02.001.

Bender, A.R., Prindle, J.J., Brandmaier, A.M., Raz, N., 2016. White matter and memory in healthy adults: coupled changes over 2 years. Neuroimage 131, 193–204. doi:10.1016/j.neuroimage.2015.10.085.

Bollen, K.A., Curran, P.J., 2006. Latent Curve Models: A Structural Equation Perspective. Wiley, Hoboken, NJ.

Cattell, R.B., Cattell, A., 1973. Measuring Intelligence with the Culture Fair Tests. Champagne, IL: Institute for Personality and Ability Testing.

Centers for Disease Control and Prevention, 2021. Diagnosed diabetes. Available at: https://www.cdc.gov/diabetes/data/statistics-report/index.html

Centers for Disease Control and Prevention, 2021. Overweight and Obesity. Available at: https://www.cdc.gov/obesity/data/prevalence-maps.html#states

Centers for Disease Control and Prevention, 2021. State Tobacco Activities Tracking and Evaluation System. Available at: https://www.cdc.gov/statesystem/index.html

Chen, J.J., Rosas, H.D., Salat, D.H., 2011. Age-associated reductions in cerebral blood flow are independent from regional atrophy. Neuroimage 55, 468–478. doi:10.1016/j.neuroimage.2010.12.032.

Chou, K.H., Wang, P.N., Peng, L.N., Liu, L.K., Lee, W.J., Chen, L.K., Lin, C.P., Chung, C.P., 2019. Location-specific association between cerebral microbleeds and arterial pulsatility. Front. Neurol 10, 1012. doi:10.3389/fneur.2019.01012.

Chung, C.P., Lee, H.Y., Lin, P.C., Wang, P.N., 2017. Cerebral artery pulsatility is associated with cognitive impairment and predicts dementia in individuals with subjective memory decline or mild cognitive impairment. J. Alzheimer's. Dis 60, 625–632. doi:10.3233/JAD-170349.

Daugherty AM & Raz, N., 2016. Accumulation of iron in the putamen predicts its shrinkage in healthy older adults: a multi-occasion longitudinal study. Neuroimage 128, 11–20. doi:10.1016/j.neuroimage.2015.12.045.

Daugherty A & Raz, N., 2015. Appraising the role of iron in brain aging and cognition: promises and limitations of MRI methods. Neuropsychol. Rev 25, 272–287. doi:10.1007/s11065-015-9292-y.

de la, Torre J.C., 2008. Pathophysiology of neuronal energy crisis in Alzheimer's disease. Neurodegener. Dis 5, 126–132. doi:10.1159/000113681.

Debette, S., Seshadri, S., Beiser, A., Au, R., Himali, J.J., Palumbo, C., Wolf, P.A., DeCarli, C., 2011. Midlife vascular risk factor exposure accelerates structural brain aging and cognitive decline. Neurology 77, 418–461. doi:10.1212/WNL.0b013e318227b227.

Ferrer E & McArdle, J.J., 2010. Longitudinal modeling of developmental changes in psychological research. Curr. Dir. Psychol. Sci 19, 149–154.

Fletcher, E., Gavett, B., Harvey, D., Farias, S.T., Olichney, J., Beckett, L., DeCarli, C., Mungas, D., 2018. Brain volume change and cognitive trajectories in aging. Neuropsychology 32, 436–449. doi:10.1037/neu0000447.

Fleysher, R., Lipton, M.L., Noskin, O., Rundek, T., Lipton, R., Derby, C.A., 2018. White matter structural integrity and transcranial Doppler blood flow pulsatility in normal aging. Magn. Reson. Imaging 47, 97–102. doi:10.1016/j.mri.2017.11.003.

Folstein, M.F., Folstein, S.E., McHugh, P.R., 1975. "Mini-mental state." A practical method for grading the cognitive state of patients for the clinician. J. Psychiatr. Res 12, 189–198.

Ghisletta, P., Mason, F., Dahle, C.L., Raz, N., 2019. Metabolic risk affects fluid intelligence changes in healthy adults. Psychol Aging 34, 912–920. doi:10.1037/pag0000402.

Gosling, R.G., King, D.H., 1974. Arterial assessment by Doppler-shift ultrasound. Proc. R. Soc. Med 67, 447–449.

Grosu, S., Rospleszcz, S., Hartmann, F., Habes, M., Bamberg, F., Schlett, C.L., Galie, F., Lorbeer, R., Auweter, S., Selder, S., Buelow, R., Heier, M., Rathmann, W., Meuller-Peltzer, K., Ladwig, K., Grabe, H.J., Peters, A., Ertl-Wagner, B.B., Stoecklein, S., 2021. Associated factors of white matter hyperintensity volume: a machine-learning approach. Sci. Rep 11, 2325. doi:10.1038/s41598-021-81883-4.

Hanon, O., Haulon, S., Lenoir, H., Seux, M.L., Rigaud, A.S., Safar, M., Girerd, X., Forette, F., 2005. Relationship between arterial stiffness and cognitive function in elderly subjects with complaints of memory loss. Stroke 36, 2193–2197. doi:10.1161/01.str.0000181771.82518.1c.

Henriksen, O.M., Jensen, L.T., Krabbe, K., Guldberg, P., Teerlink, T., Rosturp, E., 2014. Resting brain perfusion and selected vascular risk factors in healthy elderly subjects. PLoS One 9, e97363. doi:10.1371/journal.pone.0097363.

Hillman, C.H., Erickson, K,I, Kramer, A.F., 2008. Be smart, exercise your heart: exercise effects on brain and cognition. Nat. Rev. Neurosci 9, 58–65. doi:10.1038/nrn2298.

Horn, J.L., 1982. The theory of fluid and crystallized intelligence in relation to concepts of cognitive psychology and aging in adulthood. In: Craik, FI, Trehub, SE (Eds.), Aging and Cognitive Processes. Plenum Press, New York, NY, pp. 71–117.

Keage, H.A., Kurylowicz, L., Lavrencic, L.M., Churches, O.F., Flitton, A., Hofmann, J., Kohler, M., Badcock, N.A., 2015. Cerebrovascular function associated with fluid, not crystallized, abilities in older adults: a transcranial Doppler study. Psychol Aging 30, 613–623. doi:10.1037/pag0000026.

Kline, R.B., 2016. Principles and Practice of Structural Equation Modeling, 4th ed. Guilford Press, New York, NY.

Kneihsl, M., Hofer, E., Enzinger, C., Niederkorn, K., Horner, S., Pinter, D., Fandler-Höfler, S., Eppinger, S., Haidegger, M., Schmidt, R., Gattringer, T., 2020. Intracranial pulsatility in relation to severity and progression of cerebral white matter hyperintensities. Stroke 51, 3302–3309. doi:10.1161/strokeaha.120.030478.

Kyllonen, P.C ., Christal, R.E., 1990. Reasoning ability is (little more than) working-memory capacity?!. Intelligence 14, 389–433. doi:10.1016/S0160-2896(05)80012-1.

Lindenberger, U., von Oertzen, T., Ghisletta, P., Hertzog, C., 2011. Cross-sectional age variance extraction: what's change got to do with it? Psychol Aging 26, 34–47. doi:10.1037/a0020525.

Little, T.D., Jorgensen, T.D., Lang, K.M., Moore, E.G., 2014. On the joys of missing data. J. Pediatr. Psychol 39, 151–162.

MacInnes, W.D., Paull, D, Quaife, M., 1989. Longitudinal changes in regional cerebral blood flow in a normal elderly group. Arch. Clin. Neuropsychol 4, 217–226. doi:10.1093/arclin/4.3.217.

McArdle, J.J., Nesselroade, J.R., 1994. Using multivariate data to structure developmental change. In: Cohen, SH, Reese, HW (Eds.), Life-span Developmental Psychology: Methodological Contributions. Lawrence Erlbaum Associates, Hillsdale, NJ, pp. 223–267.

Müller, M., Schimrigk, K., 1994. A comparative assessment of cerebral haemodynamics in the basilar artery and carotid territory by transcranial Doppler sonography in normal subjects. Ultrasound Med Biol 20, 677–687. doi:10.1016/0301-5629(94)90025-6.

Naqvi, J., Yap, K.H., Ahmad, G., Ghosh, J., 2013. Transcranial doppler ultrasound: a review of the physical principles and major applications in critical care. Int. J. Vasc. Med 2013, 629378. doi:10.1155/2013/629378.

Nyberg, L., Boraxbekk, C.J., Sörman, D.E., Hansson, P., Herlitz, A., Kauppi, K., Ljungberg, J.K., Lövheim, H., Lundquist, A., Nordin Adolfsson, A., Oudin, A., Pudas, S., Rönnlund, M., Stiernstedt, M., Sundström, A., Adolfsson, R., 2020. Biological and environmental predictors of heterogeneity in neurocognitive ageing: evidence from betula and other longitudinal studies. Aging. Res. Rev 64, 101184. doi:10.1016/j.arr.2020.101184.

Park, D.C., Schwarz, N., 2000. Cognitive Aging: A Primer, 1st ed. Psychology Press, New York, NY.

Park, K.Y., Chung, P.W., Kim, Y.B., Moon, H.S., Suh, B.C., Yoon, W.T., 2013. Increased pulsatility index is associated with intracranial arterial calcification. Eur Neurol 69, 83–88. doi:10.1159/000342889.

Parkes, L.M., Rashid, W., Chard, D.T., Tofts, P.S., 2004. Normal cerebral perfusion measurements using arterial spin labeling: reproducibility, stability, and age and gender effects. Magn Reson Med 51, 736–743. doi:10.1002/mrm.20023.

Pase, M.P., Davis-Plourde, K., Himali, J.J., Satizabal, C.L., Aparicio, H., Seshadri, S., Beiser, A.S., DeCarli, C., 2018. Vascular risk at younger ages most strongly as-

sociates with current and future brain volume. Neurology 91, e1479–e1486. doi:10.1212/WNL.0000000000006360.
Petrenko, M., Svyrydova, N., Trufanov, Y., 2020. Susceptibility-weighted imaging and transcranial doppler ultrasound in patients with cerebral small vessel disease. Neurol. Sci 41, 2853–2888. doi:10.1007/s10072-020-04414-5.
Core Team, R ., 2016. R: A Language and Environment for Statistical Computing. Vienna, Austria. Retrieved from http://www.R-project.org
Radloff, L.S., 1977. The CES-D Scale: a self-report depression scale for research in the general population. Appl. Psych. Meas 1, 385–401.
Raz, N., 2020. Brains, hearts, and minds: trajectories of neuroanatomical and cognitive change and their modification by vascular and metabolic factors. In: Poeppel, D, Mangun, GR, Gazzaniga, MS (Eds.), The Cognitive Neurosciences. MIT Press, Cambridge, MA, pp. 61–80.
Raz, N., Lindenberger, U., 2011. Only time will tell: cross-sectional studies offer no solution to the age–brain–cognition triangle: comment on Salthouse (2011). Psychol. Bull 137, 790–795. doi:10.1037/a0024503.
Raz, N., Daugherty, A.M., Sethi, S.K., Arshad, M., Haacke, E.M., 2017. Age differences in arterial and venous cerebral blood flow in healthy adults: contributions of vascular risk factors and genetic variants. Brain Struct Funct 222, 2553–2641. doi:10.1007/s00429-016-1362-2.
Raz, N., Ghisletta, P., Rodrigue, K.M., Kennedy, K.M., Lindenberger, U., 2010. Trajectories of brain aging in middle-aged and older adults: regional and individual differences. Neuroimage 51, 501–511. doi:10.1016/j.neuroimage.2010.03.020.
Raz, N., Gunning-Dixon, F., Head, D., Williamson, A., Rodrigue, K., Acker, J.D., 2004. Aging, sexual dimorphism, and hemispheric asymmetry of the cerebral cortex: replicability of regional differences in volume. Neurobiol Aging 25, 377–396. doi:10.1016/S0197-4580(03)00118-0.
Raz, N., Lindenberger, U., Ghisletta, P., Rodrigue, K.M., Kennedy, K.M., Acker, J.D., 2008. Neuroanatomical correlates of fluid intelligence in healthy adults and persons with vascular risk factors. Cereb Cortex 18, 718–726. doi:10.1093/cercor/bhm108.
Raz, N., Lindenberger, U., Rodrigue, K.M., Kennedy, K.M., Head, D., Williamson, A., Dahle, C., Gerstorf, G., Acker, J.D., 2005. Regional brain changes in aging healthy adults: general trends, individual differences and modifiers. Cereb Cortex 15, 1676–1689. doi:10.1093/cercor/bhi044.
Raz, N., Yang, Y.Q., Rodrigue, K.M., Kennedy, K.M., Lindenberger, U., Ghisletta, P., 2012. White matter deterioration in 15 months: latent growth curve models in healthy adults. Neurobio Aging 33, 429.e1–429.e5. doi:10.1016/j.neurobiolaging.2010.11.018.
Roher, A.E., Garami, Z., Tyas, S.L., Maarouf, C.L., Kokjohn, T.A., Belohlavek, M., Vedders, L.J., Connor, D., Sabbagh, M.N., Beach, T.G., Emmerling, M.R., 2011. Transcranial doppler ultrasound blood flow velocity and pulsatility index as systemic indicators for Alzheimer's disease. Alzheimers Dement 7, 445–455. doi:10.1016/j.jalz.2010.09.002.
Rosseel, Y., 2012. lavaan: an R package for structural equation modeling. J. Stat. Softw 48, 1–36. doi:10.18637/jss.v048.i02.
Saeed, N.P., Panerai, R.B., Robinson, T.G., 2012. Are hand-held TCD measurements acceptable for estimates of CBFv? Ultrasound Med Biol 38, 1839–1844. doi:10.1016/j.ultrasmedbio.2012.05.008.
Shirahata, N., Henriksen, L., Vorstrup, S., Holm, S., Lauritzen, M., Paulson, O.B., Lassen, N.A., 1985. Regional cerebral blood flow assessed by 133Xe inhalation and emission tomography: normal values. J. Comput. Assist. Tomogr 9, 861–866.
Shrout, P.E., Fleiss, J.L., 1979. Intraclass correlations: uses in assessing rater reliability. Psychol. Bull 86, 420–428. doi:10.1037/0033-2909.86.2.420.
Sloan, M.A., Alexandrov, A.V., Tegeler, C.H., Spencer, M.P., Caplan, L.R., Feldmann, E., Wechsler, L.R., Newell, D.W., Gomez, C.R., Babikian, V.L., Lefkowitz, D., Goldman, R.S., Armon, C., Hsu, C.Y., Goodin, D.S., 2004. Assessment: transcranial Doppler ultrasonography: report of the therapeutics and technology assessment subcommittee of the american academy of neurology. Neurology 62, 1468–1481. doi:10.1212/wnl.62.9.1468.
Sugimori, H., Ibayashi, S., Ooboshi, H., Nagao, T., Fujii, K., Sadoshima, S, Fujishima, M., 1993. Age-related changes in intracranial artery velocity measured by transcranial Doppler sonography in normotensive, hypertensive and diabetic patients. Nihon Ronen Igakkai Zasshi 30, 610–616. doi:10.3143/geriatrics.30.610.
Suri, S., Chiesa, S.T., Zsoldos, E., Mackay, C.E., Filippini, N., Griffanti, L., Mahmood, A., Singh-Manoux, A., Shipley, M.J., Brunner, E.J., Kivimäki, M., Deanfield, J.E., Ebmeier, K.P., 2020. Associations between arterial stiffening and brain structure, perfusion, and cognition in the Whitehall II Imaging Sub-study: a retrospective cohort study. PLoS Med 17, e1003467. doi:10.1371/journal.pmed.1003467.
Szolnoki, Z., Somogyvári, F., Kondacs, A., Szabó, M., Fodor, L., Bene, J., Melegh, B., 2004. Specific APOE genotypes in combination with the ACE D/D or MTHFR 677TT mutation yield an independent genetic risk of leukoaraiosis. Acta. Neurol. Scand 109, 222–227.
Tarumi, T., Ayaz Khan, M., Liu, J., Tseng, B.M., Parker, R., Riley, J., Tinajero, C., Zhang, R., 2014. Cerebral hemodynamics in normal aging: central artery stiffness, wave reflection, and pressure pulsatility. J. Cereb. Blood. Flow. Metab 34, 918–971. doi:10.1038/jcbfm.2014.44.
ten Dam, V.H., van den Heuvel, D.M., de Craen, A.J., Bollen, ELEM., Murray, H.M., Westendorp, R.G.J., Blauw, G.J., van Buchem, M.A., 2007. Decline in total cerebral blood flow is linked with increase in periventricular but not deep white matter hyperintensities. Radiology 243, 198–203. doi:10.1148/radiol.2431052111.
van Es, A.C., van der Grond, J., ten Dam, V.H., de Craen, A.J., Blauw, G.J., Westendorp, R.G., Admiraal-Behloul, F., van Buchem, M.A., 2010. PROSPER Study Group. associations between total cerebral blood flow and age related changes of the brain. PLoS One 5, e9825. doi:10.1371/journal.pone.0009825.
Vernooij, M.W., van der Lugt, A., Ikram, M.A., Wielopolski, P.A., Vrooman, H.A., Hofman, A., Krestin, G.P., Breteler, M.M.B., 2008. Total cerebral blood flow and total brain perfusion in the general population: the rotterdam scan study. J. Cereb. Blood. Flow. Metab 28, 412–419. doi:10.1038/sj.jcbfm.9600526.
Vikner, T., Eklund, A., Karalija, N., Malm, J., Riklund, K., Lindenberger, U., Bäckman, L., Nyberg, L., Wåhlin, A., 2021. Cerebral arterial pulsatility is linked to hippocampal microvascular function and episodic memory in healthy older adults. J. Cereb. Blood. Flow. Metab. 41, 1778–1790. doi:10.1177/0271678X20980652.
Wardlaw, J.M., Smith, E.E., Biessels, G.J., Cordonnier, C., Fazekas, F., Frayne, R., Lindley, R.I., O'Brien, J.T., Barkhof, F., Benavente, O.R., Black, S.E., Brayne, C., Breteler, M., Chabriat, H., Decarli, C., de Leeuw, F.E., Doubal, F., Duering, M., Fox, N.C., Greenberg, S., Hachinski, V., Kilimann, I., Mok, V., van Oostenbrugge, R., Pantoni, L., Speck, O., Stephan, B.C., Teipel, S., Viswanathan, A., Werring, D., Chen, C., Smith, C., van Buchem, M., Norrving, B., Gorelick, P.B., Dichgans, M., 2013. Standards for reportIng vascular changes on neuroimaging (STRIVE v1): neuroimaging standards for research into small vessel disease and its contribution to ageing and neurodegeneration. Lancet Neurol 12, 822–838. doi:10.1016/S1474-4422(13)70124-8.
Yuan, P., Voelkle, M.C., Raz, N., 2018. Fluid intelligence and gross structural properties of the cerebral cortex in middle-aged and older adults: a multi-occasion longitudinal study. Neuroimage 172, 21–30.
Zarrinkoob, L., Ambarki, K., Wåhlin, A., Birgander, R., Eklund, A., Malm, J., 2015. Blood flow distribution in cerebral arteries. J. Cereb. Blood Flow. Metab 35, 648–654. doi:10.1038/jcbfm.2014.241.
Zhao, M., Amin-Hanjani, S., Ruland, S., Curcio, A.P., Ostergren, L., Charbel, F.T., 2007. Regional cerebral blood flow using quantitative MR angiography. Am. J. Neuroradiol 28, 1470–1473. doi:10.3174/ajnr.A0582.